Journal of Colloid and Interface Science **213,** 273–286 (1999)
Article ID jcis.1998.6036, available online at http://www.idealibrary.com on IDEAL®

Monte Carlo Simulation of Particle Aggregation and Simultaneous Restructuring

Pushkar Tandon[1] and Daniel E. Rosner[2]

Department of Chemical Engineering, Yale University, New Haven, Connecticut 06520-8286

Received May 13, 1997; accepted December 18, 1998

Ultrafine ("nano"-) particles produced from highly supersaturated vapors or liquids often undergo rapid coagulation and slow interspherule coalescence. Resulting "aggregates" typically contain hundreds of small spherules bound together in tenuous structures characterized by mass fractal dimensions much less than 3. Such aggregates have large and relatively accessible initial surface area but are metastable with respect to more compact configurations, especially in high temperature environments (e.g., flames). Subject to deliberately idealized "uncoupled" rate laws for coagulation and coalescence, we illustrate the power of Monte Carlo simulation methods to obtain the self-preserving joint distribution function (with respect to both particle size and surface area) of populations of coagulating fractal aggregates in the continuum regime, simultaneously undergoing finite-rate restructuring (e.g., via surface-energy-driven viscous flow). Unconditional distributions with respect to either particle volume or area are also obtained from the Monte Carlo simulations. These are conveniently quantified by fitting them to log-normal distributions and we report the sensitivity of the associated spreads to characteristic fusion/coagulation time ratio, χ, and particle fractal dimension, D_f, here prespecified. We also calculate and report selected "mixed" moments of the joint pdf with respect to particle volume and surface area needed for engineering calculations of deposition or diffusion-controlled vapor scavenging, as well as the important ratio of actual mean area to that area corresponding to the mean particle volume in the aerosol population. This work sets the stage for tractable simulations of particle dynamics in more complex coagulating systems requiring multi-internal (state-) variables for their more realistic and self-consistent description.

Key Words: **aggregate coagulation; aggregate sintering; bi-variate population balance; Monte Carlo simulation; self-preserving distributions; aerosol dynamics.**

1. INTRODUCTION AND OBJECTIVES

1.1. Fractal Aggregates Resulting from Coagulation

Many early studies of coagulation processes explicitly or implicitly assume that the coalescence (or, more generally, restructuring) rate of the coagulating particles is rapid enough to give rise to uniform density fully "coalesced" spherical particles. But, in many technologies, aggregates comprised of large numbers of spherules ("primary" particles) which have coagulated but not coalesced are observed. Moreover, each of these often has the useful property that the number of spherules scales with a power, D_f, less than three, of the radial distance from the aggregate center-of-mass.[3] In a wide variety of aggregate–aggregate coagulating systems (physically or optically sampled), as well as computer simulations of Brownian coagulation without post-collision restructuring, D_f has been observed to be near 1.7 ± 0.1 (12, 41, 51, 53), but probably because of partial restructuring, laboratory-produced aggregates have been reported with intermediate D_f values, e.g., 2.2 for small silver aggregates (37). The fractal dimension 2.5 has been reported in systems with aggregate–monomer coagulation, e.g., metal oxides produced by spray-precipitation–oxidation in the seeded premixed flame experiments of Matsoukas and Friedlander (20). This "spectrum" of observed morphologies suggests that, in general, one must consider intermediate degrees of coalescence, i.e., the consequences of finite rate coalescence in coagulating systems (13), but introducing a simulation method better suited to such multivariate problems than moment methods or finite-difference methods (56). The competition between coagulation and coalescence rates is also decisive in determining observed spherule ("primary" particle) sizes (54, 17) and, hence, specific surface area.

1.2. Theories of Aggregate Restructuring Kinetics

Multispherule fractal aggregates are metastable with respect to more compact configurations and in certain environments will exhibit finite-rate sintering or restructuring (see, e.g., Refs. 11, 51). The observed extent of restructuring in any system will depend on the relative magnitude of characteristic times for sintering, coagulation, and flow, since these rate processes generally occur simultaneously.

[1] Present address: Corning Inc., Corning, NY 14831.

[2] To whom all correspondence should be addressed. E-mail: daniel.rosner@qm.yale.edu.

[3] The scaling exponent is the so-called fractal dimension, D_f; see, e.g., Koylu *et al.* (14).

0021-9797/99 $30.00

Aggregate restructuring itself can be due to one or more various mechanisms, such as surface-energy driven viscous flow sintering (13, 45, 1) volume and/or surface diffusion (12, 51, 48), interparticle forces (4, 24), carrier fluid induced shear (27), Brownian restructuring of "dry" granular aggregates (48, 58), or capillary condensation (37, 19), etc. Despite increasing activity, accurate rate laws for restructuring by these mechanisms are not yet available for large multispherule aggregates. However, we can illustrate the most important features of the versatile Monte Carlo (MC) simulation method emphasized here by merely invoking a restructuring law based on long time sintering behavior of two spherules, as reviewed by Koch and Friedlander (13) and treating the fractal dimension as though it were an independently specified parameter.

1.3. Self-Preserving Behavior for Particle Size and Area Distributions

For $D_f = 3$, Schumann (38) and for more realistic collision kernels, Swift and Friedlander (43) have shown that size distribution of coagulating spherical aerosol particles tends to an asymptotic shape for a variety of situations of practical interest. This self-preserving behavior with respect to size for Brownian coagulation in the continuum regime for dense spherical particles ($D_f = 3$) has been studied extensively. Swift and Friedlander (43) introduced a similarity transformation into the coagulation equation to establish the nature of the integro-ordinary differential equation (IODE) satisfied by the self-preserving distribution. Friedlander and Wang (8) successfully obtained a finite-difference numerical solution to be similarity-transformed coagulation equation. Alternatively, Lee (16) presented a moment method analysis to obtain the asymptotic spread for approximately log-normal distributions. The corresponding cases for coagulating fractal aggregates has received less attention (59, 57). In the above-mentioned studies, the effect on the population distribution of particles of finite-rate coalescence (restructuring) has been neglected. Here for the first time we address the question of self-preserving behavior for bivariate populations of fractal aggregates coagulating as a result of Brownian motion in the continuum regime and, simultaneously, undergoing finite rate-restructuring. While some of our present simplifying assumptions will have to be relaxed, even our present results for these bivariate population distributions are of potential interest for a number of applications. For example, certain moments of these distribution functions are needed to predict total mass deposition rates on surfaces of particles that have coagulated in the mainstream (30, 34, 47), the accessible surface area of aerosol populations exchanging heat or mass with their host (carrier) gas (33), loss of accessible area with time of coagulating populations because of diffusional limitations, etc.

1.4. Monte Carlo Simulation Methods

Regarding computational methods, Meakin (21) suggested an interesting Monte Carlo method to simulate the evolution of particle populations governed by the Smoluchowski equation. We here use an extension of this method to generate for the first time the joint pdf between particle volume and area and then investigate the sensitivity of the self-preserving spread parameters (for particle size and surface area) to both aggregate fractal dimension (59) and characteristic fusion time for aggregate populations coagulating by Brownian diffusion in the continuum (Kn $\ll$ 1 or high pressure) regime. Corresponding MC calculations in the free-molecular regime are now in progress and will be presented elsewhere Tandon *et al.* (49). We argue that MC-based methods are particularly well suited to such multivariate coagulation problems and will lend themselves to extensions to include more complete rate laws and the inclusion of additional particle state variables.

For illustrative purposes, and in the absence of accepted fully coupled rate laws, we exploit the simple "uncoupling" approximation of Koch and Friedlander (13); viz, the collision rate dynamics are considered to be unaltered by the surface areas of the colliding particles. The corresponding self-preserving joint pdf between particle area and volume will be needed, among other things, for developing moment method solutions for two-internal variable population balance equations. Our MC results for unconditional distributions with respect to size (aggregate volume) are independently checked by comparing them with those previously obtained by finite-difference solutions of the similarity transformed coagulation equation (8, 44).

2. MATHEMATICAL MODEL

For a fractal aggregate,[4] taking particle volume and surface area as continuous variables, an aggregate distribution function $n(v, a)$ can be defined such that the particle number density having volumes between v and $v + dv$ and surface areas between a and $a + da$ is

$$dN_p = n(v, a)dvda. \qquad [1]$$

In a nonflow, spatially homogeneous system, the rate of change of $n(v, a)$ is given by the sum of two contributions (13, 56):

$$\frac{\partial n(v, a)}{\partial t} = \left(\frac{\partial n(v, a)}{\partial t}\right)_{coag} + \left(\frac{\partial n(v, a)}{\partial t}\right)_{fusion}. \qquad [2]$$

The first term on the right-hand side is the change in the distribution function as a result of Brownian coagulation, i.e.,

[4] For an aggregate, the fractal dimension may be defined as $D_f = d(\ln N_{prim})/d(\ln r)$ where N_{prim} is the expected number of "primary" particles (spherules) contained within a sphere of radius r measured from the aggregate center of mass.

$$\left[\frac{\partial}{\partial t}n(v,a)\right]_{\text{coag}} = \frac{1}{2}\int_0^v \theta\left(a > \left(\frac{v'}{v_1}\right)^{2/3}a_1 + \left(\frac{v-v'}{v_1}\right)^{2/3}a_1\right) \times \int_{(v'/v_1)^{2/3}a_1}^{(v'/v_1)a_1} \beta(v', v-v'; (a', a-a')) \times n(v', a')n(v-v', a-a')(da') \times dv' - n(v,a)\cdot\int_0^\infty \int_{(\bar{v}'/v_1)^{2/3}a_1}^{(v'/v_1)a_1} \times \beta(v, v'; (a, a'))n(v', a')(da')dv', \quad [3]$$

where θ is the step function and v_1 and a_1 are "primary" particle volume and surface area, respectively. For simplicity and to illustrate our methodology, the collision frequency (rate constant), $\beta(u, v)$, between aggregates of sizes u and v is here considered to be only a function of particle size (volume) and not of aggregate surface area, and for aggregates undergoing Brownian coagulation in the continuum regime is taken to be[5]

$$\beta(u, v) = K\cdot\left(\frac{1}{u^{1/D_f}} + \frac{1}{v^{1/D_f}}\right)\cdot(u^{1/D_f} + v^{1/D_f}), \quad [4]$$

where K is an environment-dependent proportionality constant (see Nomenclature). To derive the above relation, it is assumed that in the continuum regime, both mobility and collision diameters are simply proportional to the aggregate radius of gyration, R_g. The systematic reductions in mobility diameter associated with the nonzero and spatially variable permeability of aggregates (46) is neglected, since these effects are expected to be small in the continuum regime, especially for large ($N_{\text{prim}} \gg 1$) aggregates.

The second term on the right-hand side of Eq. [4] is the result of particles undergoing restructuring and can be written

$$\left(\frac{\partial n(v,a)}{\partial t}\right)_{\text{fusion}} = \frac{\partial}{\partial a}[\dot{a}n(v, a, t)]. \quad [5]$$

Whatever the local environment, the rate of change of area with time for an individual aggregate, $\dot{a}$, depends on the mechanism of restructuring. Based on the long time sintering behavior of two spherules, Koch and Friedlander (13) suggested the following linearized expression for the rate of surface area reduction,

$$\dot{a} = -\frac{1}{t_f}\cdot(a - a_{\text{final}}), \quad [6]$$

where a_{final} is the area of the fully compacted sphere ($\pi(6v/\pi)^{2/3}$) and the characteristic time of fusion/sintering, t_f, for viscous flow sintering, is found to be

$$t_f = \frac{\mu R_1}{\sigma}. \quad [7]$$

In Eq. [7] μ is the spherule viscosity and σ is the particle surface energy. The characteristic time t_f here is considered to be time-independent, even though these laws are sometimes applied to restructuring aggregates of complex morphology with $R_{1,\text{eff}}$ taken to be proportional to the instantaneous v/a (56). Restructuring of aggregates, in general, also results in an increase in fractal dimension (see, e.g., Ref. 46), a fact which will have to be incorporated in future applications of our MC method. Moreover, our pseudo-homogeneous methods applied to large aggregates with $D_f > 2$ (46) have revealed that the aggregate area reduction rate not only is quite different from the two-sphere sintering behavior considered here, but besides surface area, is also a function of aggregate size. Relaxing these oversimplifying assumptions (work in progress) is likely to preclude existence of a "self-preserving" solution with formally prespecified D_f (see below). However, even in such situations, our present simulation methods will remain valid for predicting the evolution of aggregating–restructing populations. Furthermore, Monte Carlo methods are versatile enough to handle complex coupling between the coagulation and fusion terms in solving the population balance equation. The characteristic fusion times for some of the other restructuring mechanisms are as follows:

Bulk diffusion:

$$t_f = \frac{k_B T(R_1)^3}{12 D_v v_m \sigma} \quad [8]$$

Surface diffusion (e.g., Ref. 23):

$$t_f = \frac{k_B T(R_1)^4}{24 D_s v_m \sigma \delta}, \quad [9]$$

where k_B is the Boltzmann constant, D_v and D_s are, respectively, the volume and surface diffusion coefficients, v_m is the molecular volume, and factor δ is a surface diffusion layer thickness, approximately equal to $3(6v_m/\pi)^{1/3}$. The increased sensitivity to spherule size is noteworthy, with possible consequences investigated further in Section 4.2.

For an aggregate population with distribution function $n(v, a)$, the total aggregate number density, N_p, and volume fraction, ϕ, are

[5] This approximate use of the gyration radius as an effective radius for mobility and collision for fractal-like aggregates has been demonstrated to be successful in the recent near free-molecule limit optical experiments of Oh and Sorensen (25).

$$N_p = \int_0^\infty \int_0^\infty n(v, a)dvda \qquad [10]$$

and

$$\phi = \int_0^\infty \int_0^\infty vn(v, a)dvda \qquad [11]$$

and the ratio of ϕ and N_p gives the average aggregate volume, $\bar{v}$ in the distribution. Likewise, the average aggregate area is defined as

$$\bar{a} \equiv \frac{\int_0^\infty \int_0^\infty an(v, a)dvda}{N_p}. \qquad [12]$$

We now define the similarity-transformed particle state variables as

$$\eta_1 \equiv v/\bar{v}; \quad \eta_2 \equiv a/\bar{a} \qquad [13]$$

and define the corresponding dimensionless *pdfs* as

$$\psi_1 \equiv \frac{\bar{v}}{N_p}\frac{\partial N_p}{\partial v}; \quad \psi_2 \equiv \frac{\bar{a}}{N_p}\frac{\partial N_p}{\partial a} \quad \text{and}$$

$$\psi_{12} \equiv \frac{\bar{a}\bar{v}}{N_p}\frac{\partial^2 N_p}{\partial v \partial a} = \frac{\bar{v}\bar{a}n(v, a)}{N_p}, \qquad [14]$$

where ψ_{12} is clearly the dimensionless joint pdf $n(v, a, t)$ between particle volume and area. The behavior of the bivariate distribution function, here economically described via $\psi_{12}(\eta_1, \eta_2)$, is needed in many applications (see Section 4.3) and numerical simulation results will also be useful in developing moment method approximate solutions to the population balance equation with two internal variables (e.g., size and surface area). We are also interested in several dimensionless partial moments[6] of $\psi_1(\eta_1)$, $\psi_2(\eta_2)$; in particular,

$$\mu_k \equiv \int_0^\infty \eta_1^k \psi_1(\eta_1)d\eta_1 \quad (k = 0, 1, 2, 3, \ldots, 1/D_f, \text{etc}) \qquad [15]$$

as well as certain mixed moments (see Section 4.3 below). While it is straightforward to prove the existence of self-preserving behavior with respect to volume for our choice of rate laws governing coagulation frequency (Eq. [4]) and surface area reduction (Eq. [6]), self-preserving behavior with respect to area is empirically established here by comparing the solution (Section 3) at two different times (at 2×10^5 and 3×10^5 Monte Carlo time steps). More realistic coagulation and sintering laws will, in general, preclude the existence of a self-preserving solution, but our MC-based methods will still be applicable to simulate the aggregate population dynamics. We now proceed to find the relationship between $\psi_1(\eta_1)$, $\psi_2(\eta_2)$, and $\psi_{12}(\eta_1, \eta_2)$, i.e., the relevant distribution functions in the so-called self-preserving or long-time limit.

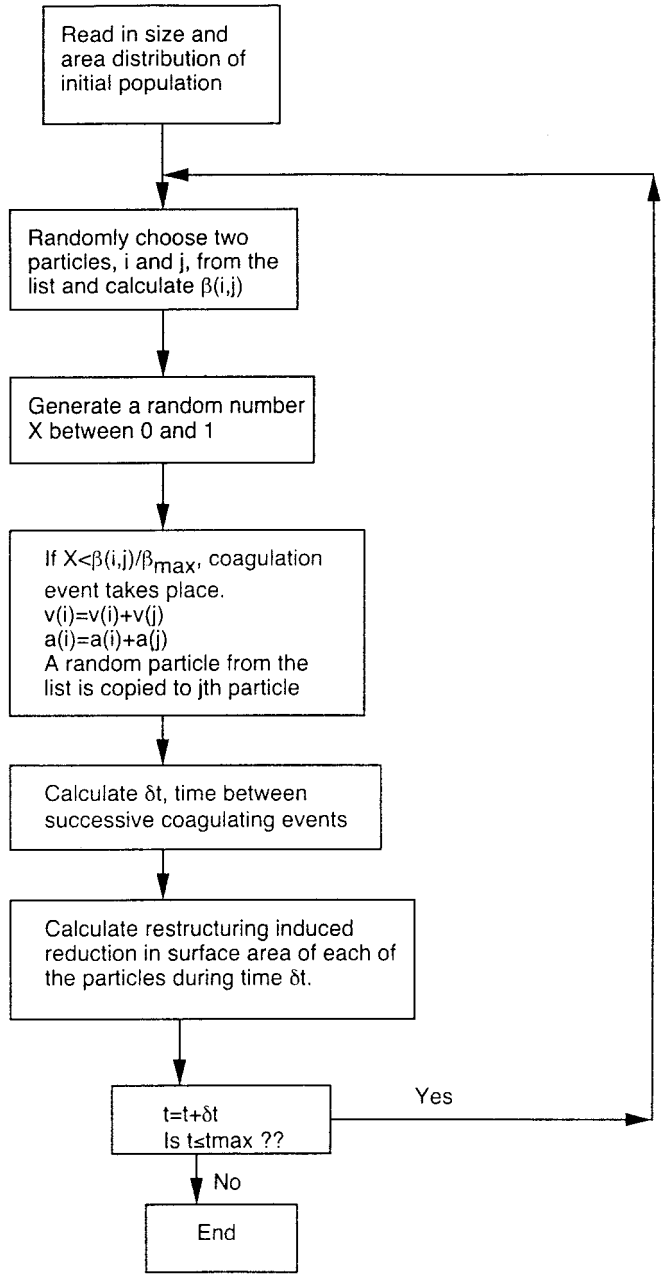

FIG. 1. Flowchart of the Monte Carlo algorithm used to simulate the self-preserving distributions with respect to particle volume and surface area.

[6] Applications in which mixed moments are required will be considered in our future work; see, also, Section 4.3 and Deimer and Olson (6).

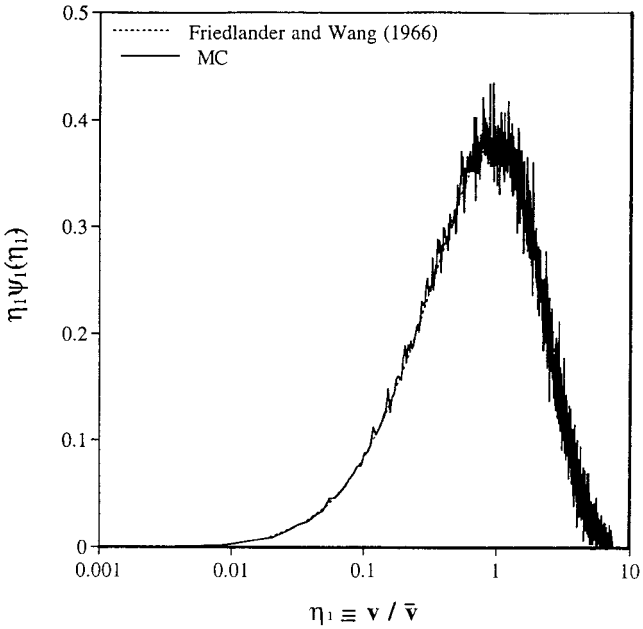

FIG. 2. Self-preserving size distribution using present Monte Carlo method, and finite-difference numerical solution (8) for $D_f = 3$; continuum Brownian coagulation.

3. MONTE CARLO SIMULATION OF POPULATION BALANCE EQUATION

A number of alternative Monte Carlo algorithms have been proposed to solve the Smulochowski equation (Eq. [3], but with a single internal variable) (42, 9, 40). A rather simple algorithm (quite similar to the Metropolis algorithm for calculating equilibrium properties of a gas (2) was suggested by Meakin (21). We here use a variant of this algorithm to solve the particle dynamics equation (Eq. [2]) for coagulating particles undergoing finite-rate coalescence. A flowchart of the algorithm is shown in Fig. 1. We consider, say, $N = 10^4$ particles in our system, each of unit volume and surface area. Two particles, i and j, are selected randomly from the list and the collision frequency function $\beta(v_i, v_j)$ is evaluated. A random number X between 0 and 1 is generated and if this number is smaller than $\beta(v_i, v_j)/\beta_{max}$, the two particles are combined to form a particle with volume $v_i + v_j$ and surface area $a_i + a_j$; otherwise they are returned back to their original positions. β_{max} is the maximum value of $\beta(v_i, v_j)$ for any pair of objects on the list. The time between successive coagulation events is calculated as

$$\Delta t = \frac{1}{\beta_{max} N_p}. \qquad [16]$$

While the above expression will suffice for our present needs, more refined methods to obtain Δt have recently been used by Smith and Matsoukas (40). Equation [6] is integrated to obtain the surface area reduction of each of the particles during the time interval between successive coagulation events. Whenever a successful collision takes place, a particle is picked at random from the list and is copied to the vacant site created because of the successful collision. It can be shown that this does not effect the self-preserving size distribution. The simulations were carried over a large number of steps (200,000) for the distribution to reach self-preserving behavior. Results were averaged over a large number of simulations (15) to reduce the statistical noise inherent in Monte Carlo methods. Each simulation (for 200,000 steps) took about 2 h CPU on a Sparc-10 workstation.

4. RESULTS AND DISCUSSION

4.1. Distribution with Respect to Size (Irrespective of Area)

Because of the collision (coagulation) rate law (Eq. [6]) chosen for our simulations (frequency independent of particle surface area) and our prespecification of the fractal dimension D_f, new results for the unconditional distribution with respect to size are necessarily identical to results for the case when no restructuring was considered in determining the self-preserving behavior (44). In Fig. 2, we plot the self-preserving distribution obtained from Monte Carlo simulations for $D_f = 3$ (corresponding to $\chi \to 0$) and the corresponding finite-difference continuum results of Friedlander and Wang (8). In Figs. 3–4, are shown the corresponding self-preserving distributions using Monte Carlo simulations with the specified fractal dimensions, $D_f = 2.5$ and 2.18. Also shown in these figures is the

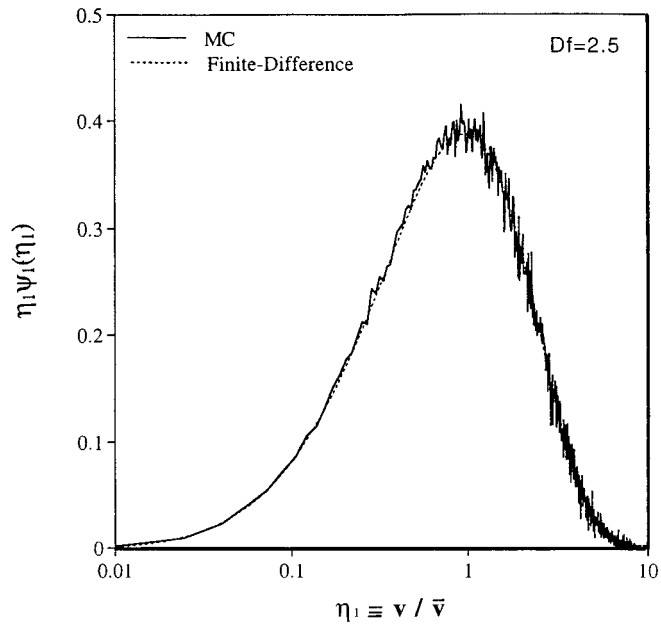

FIG. 3. Self-preserving size distribution using present Monte Carlo method and finite-difference numerical solution for $D_f = 2.5$; continuum Brownian coagulation.

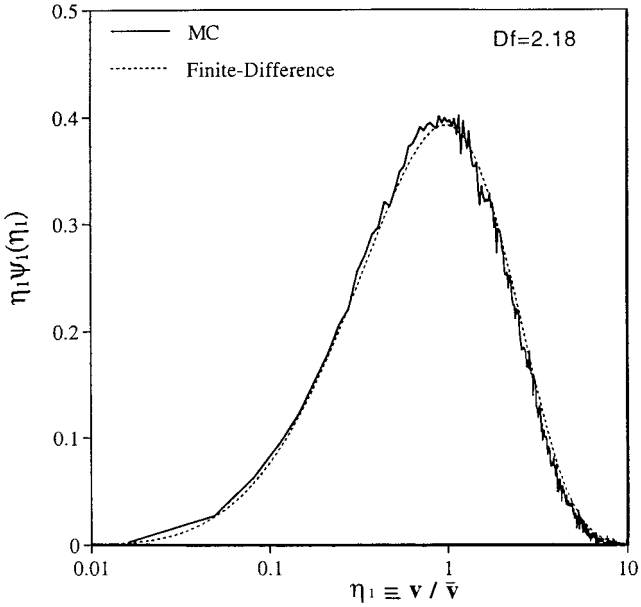

FIG. 4. Self-preserving size distribution using Monte-Carlo method and finite-difference numerical solution for $D_f = 2.18$; continuum Brownian coagulation.

numerical solution of the similarity transformed population balance equation (see Ref. 44 for details of the numerical solution). All solutions using the Monte Carlo method are clearly in excellent agreement with the finite-difference numerical solution. Based on the distributions calculated, the standard deviation, $\sigma_{g,v}$ (Eq. [5] of Ref. 28), and some relevant moments[7] have been computed and are reported in Tables 1 and 2, respectively. Since the calculated distributions are nearly log-normal (note small departures from Gaussian behavior for $\eta_1\psi_1$ vs $\log_{10}\eta_1$), the population spread, $\sigma_{g,v}$, can be defined as (29, 15)

$$\ln^2(\sigma_{g,v}) = \int_0^\infty \left(\ln\left[\frac{\eta_1 \bar{v}}{v_g} \right] \right)^2 \cdot \psi_1 d\eta_1, \qquad [17]$$

where v_g is the geometric mean size of the distribution

$$\ln(v_g) = \int_0^\infty \ln(\eta_1 \bar{v}) \cdot \psi_1 d\eta_1. \qquad [18]$$

As a further check, the distributions calculated were found to satisfy to within 1% the required normalization relations,

$$\int_0^\infty \psi_1(\eta_1) d\eta_1 = 1 \quad \text{(i.e., } \mu_0 = 1\text{)}$$

and

$$\int_0^\infty \eta_1 \psi_1(\eta_1) d\eta_1 = 1 \quad \text{(i.e., } \mu_1 = 1\text{)}. \qquad [19a,b]$$

The distribution also corresponds well with some of the moments reported earlier in the literature (see Table 2) (30). Interestingly, the continuum limit asymptotic spread parameter is observed to decrease slightly with a decrease in specified aggregate fractal dimension. Thus, we find that $\sigma_{g,v}$ slowly decreases from the value of 2.98 for $D_f = 3$ to 2.7 for $D_f = 1.8$—a trend quite different from that found in the free molecular limit by Wu and Friedlander (59). The spreads reported are also in agreement with those reported by Vemury and Pratsinis (57).

A rather different approach can also be used to verify these interesting continuum-regime monodispersity trends with decreasing prespecified fractal dimension. If in the spirit of Lee *et al.* (16), we assume initially log-normal distributions (of arbitrary spread $\sigma_{g,v}$) and that log-normality of the distribution is approximately maintained at all times during coagulation, using a moment method analysis, the standard deviation, $\sigma_{g,v}$, can be shown to satisfy the nonlinear ODE (44),

$$\frac{d\sigma_{g,v}}{d\tau} = \frac{[\exp(\{\ln \sigma_{g,v}\}^2) - 2]\left[1 + \exp\left(\left\{ \frac{\ln \sigma_{g,v}}{D_f} \right\}^2 \right) \right]}{(\ln \sigma_{g,v})\exp(\{\ln \sigma_{g,v}\}^2)[\exp(\{\ln \sigma_{g,v,0}\}^2) - 2]} \cdot \sigma_{g,v}, \qquad [20]$$

where $\tau = KN_{p,t=0}t$. Equation [20] was integrated numerically for different values of $\sigma_{g,v,0}$ until τ was large enough for $\sigma_{g,v}$ to the self-preserving limit, independent of $\sigma_{g,v,0}$. Asymptotic population spread parameters $\sigma_{g,v}$ calculated in this way are considerably smaller than those obtained from MC and numerical calculations. However, all of the above-mentioned methods

TABLE 1

Predicted Self-Preserving Particle Size Distribution Spreads of Populations Coagulating Due to Brownian Motion in the Continuum Regime, as Calculated by Monte Carlo Method

D_f	σ_g
3	2.98
2.5	2.87
2.18	2.80
1.8	2.69

[7] The moments can be used to define alternative spread parameters via the log-normal interrelation: $\mu_k = \exp[(k(k-1)/2)\ln^2\sigma_g]$.

TABLE 2

Selected Dimensionless Moments (with Respect to Volume) of the Unconditional Self-Preserving Size Distributions, $\psi_1(\eta_1)$, as Obtained Using the Monte Carlo Simulation Method; Continuum Limit (cf. Eq. [19])

	$D_f = 3$	$D_f = 2.5$	$D_f = 2.18$	$D_f = 1.8$	Relevance
μ_0	0.989	1.0064	1.0013	1.001	Normalization condition
μ_1	0.988	1.003	1.0046	0.999	Normalization condition
$\mu_{1/Df}$	0.904	0.9053	0.9068	0.91	Appears in ODE for $N_p(t)$
$\mu_{-1/Df}$	1.259	1.323	1.3833	1.48	Appears in ODE for $N_p(t)$
$\mu_{1-1/Df}$	0.898	0.909	0.908	0.855	Thermophoretic deposition
$\mu_{1-2/Df}$	0.894	0.933	0.969	1.015	Thermophoretic deposition
$\mu_{0.78}$ (Ref. 30)	0.924				Deposition by continuum diffusion across laminar boundary layers
$\mu_{0.78}$	0.917				
$\mu_{0.77}$ (Ref. 30)	0.922				Deposition by continuum diffusion across turbulent boundary layers
$\mu_{0.77}$	0.914				
$\mu_{0.63}$ (Ref. 57)				0.916	Deposition by continuum diffusion across laminar boundary layers
$\mu_{0.63}$				0.915	
$\mu_{0.61}$ (Ref. 57)				0.914	Deposition by continuum diffusion across turbulent boundary layers
$\mu_{0.61}$				0.913	

agree in that the continuum level self-preserving size spread is relatively insensitive to fractal dimension. The self-preserving spread, $\sigma_{g,v}$, using the approximate moment method are found to be within 1% of value of 2.3 for various values of D_f between 1.8 and 3.

4.2 "Unconditional" Distribution with Respect to Aggregate Surface Area (Irrespective of Volume)

While, because of our assumptions, ψ_2 depends only on $\eta_2 \equiv a/\bar{a}$, our results are, of course, sensitive to the basic time constant ratio: $\chi \equiv t_f/(KN_{p,0})^{-1}$. While it is straightforward to rigorously establish the existence of the self-preserving solution with respect to size for the present collision frequency law, the effective existence for rescaled surface area $a/\bar{a}(t)$ will be established here by simply comparing the distributions at two different times (corresponding to, say, 200,000 and 300,000 Monte Carlo time steps). In Figs. 5–7 we present the predicted self-preserving distribution with respect to surface area for the prespecified fractal dimensions $D_f = 2.5$, 2.18, and, formally,[8] for $D_f = 1.8$. In Fig. 5a are shown the distributions at 200,000 MC steps (corresponding to 1.51×10^4 characteristic coagulation times), while the distributions at 300,000 MC time steps ($t/(KN_{p,o})^{-1} = 1.78 \times 10^4$) are shown in Fig. 5b. Owing to the MC noise, the agreement is clearest with respect to spread. Indeed, the calculated $\eta_2\psi_2$ distributions were fit to log-normal distributions, with the estimated standard deviations reported in Table 3. Irrespective of dimensionless time, the MC-calculated distributions satisfy to within about 3% the required normalization conditions:

$$\int_0^\infty \psi_2(\eta_2)\, d\eta_2 = 1 \qquad [21]$$

$$\int_0^\infty \eta_2\psi_2(\eta_2)\, d\eta_2 = 1. \qquad [22]$$

The predicted spreads of the distribution with respect to surface area, $\sigma_{g,a}$, are seen to increase at slower relative coalescence rates, i.e., increase with the coalescence–coagulation time ratio parameter, χ ($10^2 < \chi < 10^5$), and these distributions become somewhat narrower as the prespecified fractal dimension decreases. Again, we see that, according to the present simple model the spreads with respect to surface area are relatively insensitive to aggregate morphology for Brownian continuum regime coagulation, but, as expected, are highly sensitive to the characteristic fusion/coagulation time parameter χ.

The results presented in Figs. 5–7 assume that the characteristic fusion time t_f (or time ratio χ) remains constant during the aggregation process. However, in general, t_f is a function of time through its dependence on primary particle diameter (see Eqs. [7]–[9]). We investigated this dependence by calculating instantaneous spherule diameter as $6v(t)/a(t)$. To our surprise, the resulting distributions were not sensitive to this allowance for the evolution of effective spherule diameter for the range of conditions we investigated (high χ), even for the case of surface diffusion (where the characteristic fusion time varies as

[8] See Oh and Sorensen (25) for a critical discussion of the functional form of the collision frequency expression when D_f passes through the singular value 2.

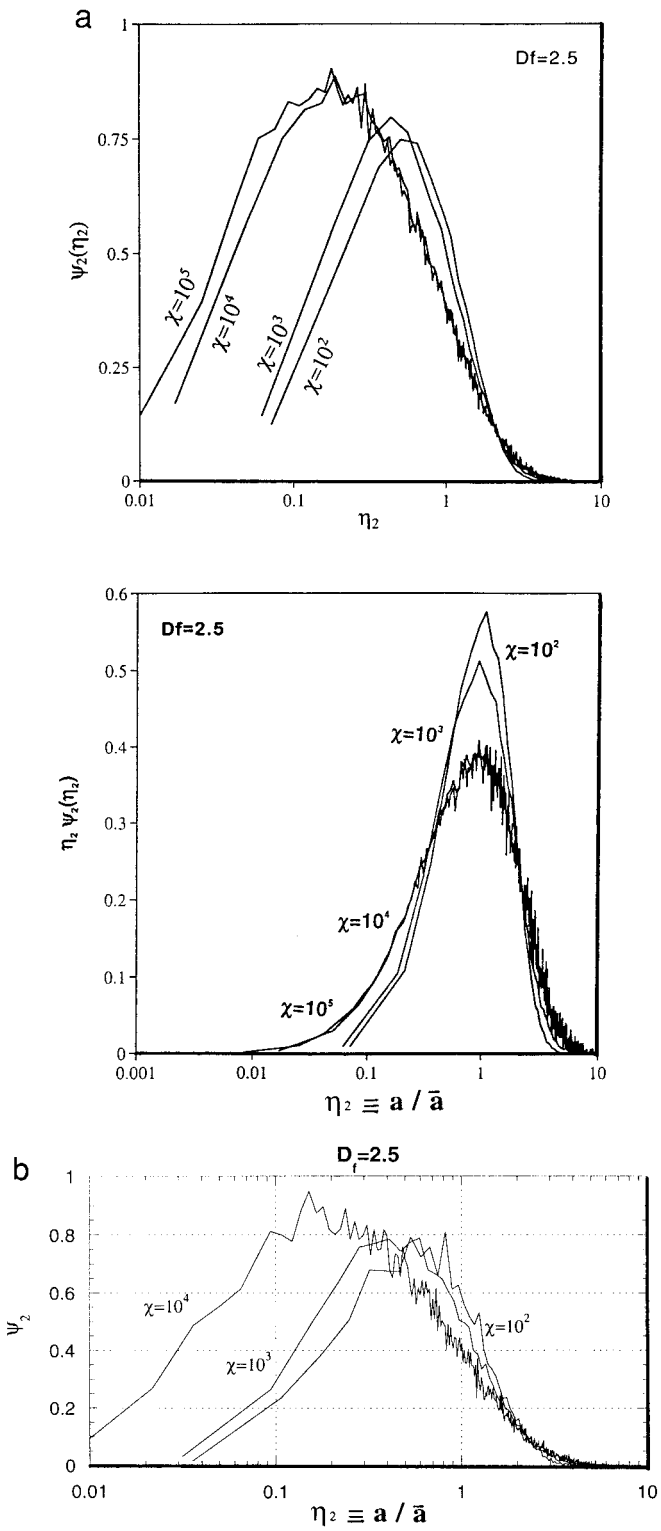

FIG. 5. (a) Self-preserving distribution with respect to the surface area for different values of the dimensionless coalescence/coagulation time ratio parameter χ ($D_f = 2.5$; 200,000 MC steps); linearized coalescence rate law and Brownian coagulation in the continuum limit. (b) Self-preserving unconditional number distribution with respect to surface area, $\psi_2(\eta_2)$, for different values of the coalescence/coagulation time ratio parameter χ ($D_f = 2.5$, 300,000 MC steps); linearized coalescence rate law and Brownian coagulation in the continuum limit.

the fourth power of particle diameter). In Fig. 8a, the distributions are shown for $[\chi]_{t=0} = 10^5$, while the distributions for $[\chi]_{t=0} = 10^5$ are shown in Fig. 8b. The sensitivity to the particle diameter evolution may be more pronounced for the time taken to reach the self-preserving distribution, an important time lag currently under investigation.

We also investigated the evolution of the dimensionless area ratio parameter $\bar{a}/a_{min}(\bar{v})$ during the course of aggregation–restructuring. This area ratio parameter was found to asymptotically approach values relatively independent of time ratio parameter χ and D_f for $\chi < 10^3$ and a strong function of fractal dimension D_f above $\chi = 10^3$. Asymptotic values of this area ratio parameter for different combinations of D_f and χ are reported in Table 4. This ratio is closely related to the population average parameter $\langle t_f \rangle$ defined by $[\bar{a} - a_{min}(\bar{v})]/(-\dot{\bar{a}})$ for the evolving population. This is an extremely important quantity since experimental inferred t_f values based on restructuring measurements (52) are necessarily based on population averages rather than observations on any one aggregate. Methods to obtain t_f from observations of $\langle t_f \rangle$ are under development and will be presented elsewhere.

4.3. Joint pdf with Respect to v and a: $\psi_{12}(\eta_1, \eta_2)$

A representative plot for the joint distribution function $\psi_{12}(\eta_1, \eta_2)$ for $D_f = 2.5$ and $\chi = 10^3$ is shown in Fig. 9, although for this oversimplified choice of coagulation and coalescence (β, $\dot{a}$) rate laws. The number of particles (10,000) considered in our simulations is somewhat small to sample the complete η_1 and η_2 space accurately, but should prove adequate for estimating the mixed moments (weighted integrals). Moreover, the results presented should provide important trends and approximate distribution shapes. The spreads and distributions calculated can also be used to guide the development of moment method approximate solutions for the population balance equation with size and surface area as internal variables (6); however, future work will have to consider more realistic and inevitably coupled (β, $\dot{a}$) rate laws, perhaps treating D_f as a state variable rather than a prespecified parameter. Based on the calculated distributions for the present idealized model, we also calculate the mixed moments, μ_{kl}, of the joint probability density function, $\psi_{12}(\eta_1, \eta_2)$ as

$$\mu_{kl} \equiv \int_0^\infty \int_0^\infty \eta_1^k \eta_2^1 \psi_{12}(\eta_1, \eta_2) d\eta_1 d\eta_2. \qquad [23]$$

The mixed moments[9] are shown as a surface in Fig. 10 in the domain $-2 < (k, l) < 2$ for six combinations of the pre-specified parameters χ and D_f. Some of the nonunity

[9] It is interesting that important dimensionless ratios, such as the area ratio parameter defined and reported in Section 4.2, cannot be written in terms of one or more of the mixed moments discussed above.

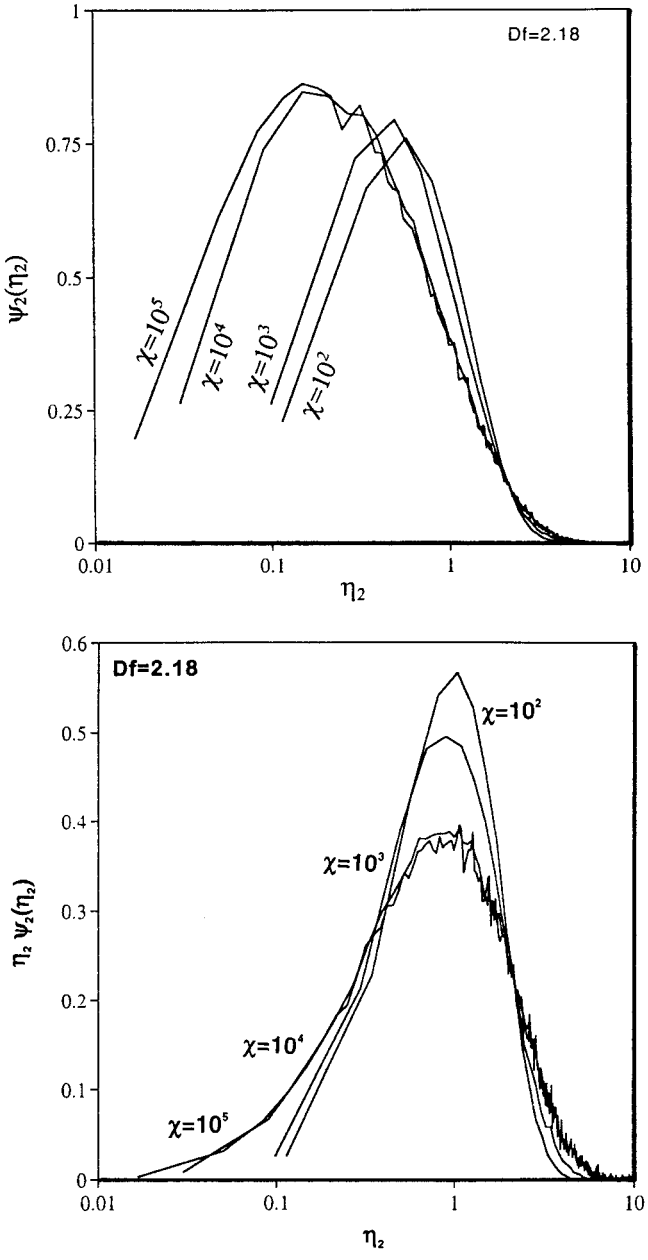

FIG. 6. Self-preserving distribution with respect to the surface area for different values of the dimensionless coalescence/coagulation time ratio parameter χ ($D_f = 2.18$); linearized coalescence rate law and Brownian coagulation in the continuum limit.

important mixed moments of physical interest include $\mu_{2/3,0}$ and $\mu_{0,1/2}$, needed for predicting the evolution of mean area of the population and diffusion-controlled vapor scavenging rates (31), respectively. These moments can be used, among other things, to predict the structure of multiphase boundary layers and mixing, once current research reveals more about the transport properties of aggregated particles (see, e.g., (46).

Monte Carlo methods, besides being easy to implement, also provide tractable means for solving population balance equations with multi-internal variables (a conclusion independently reached by Gooch and Hounslow (10) for crystallization applications). These methods, applied here for the simplest case of spatially homogeneous coagulation and simultaneous but "uncoupled" rate processes, can now be extended in solving the generalized population balance

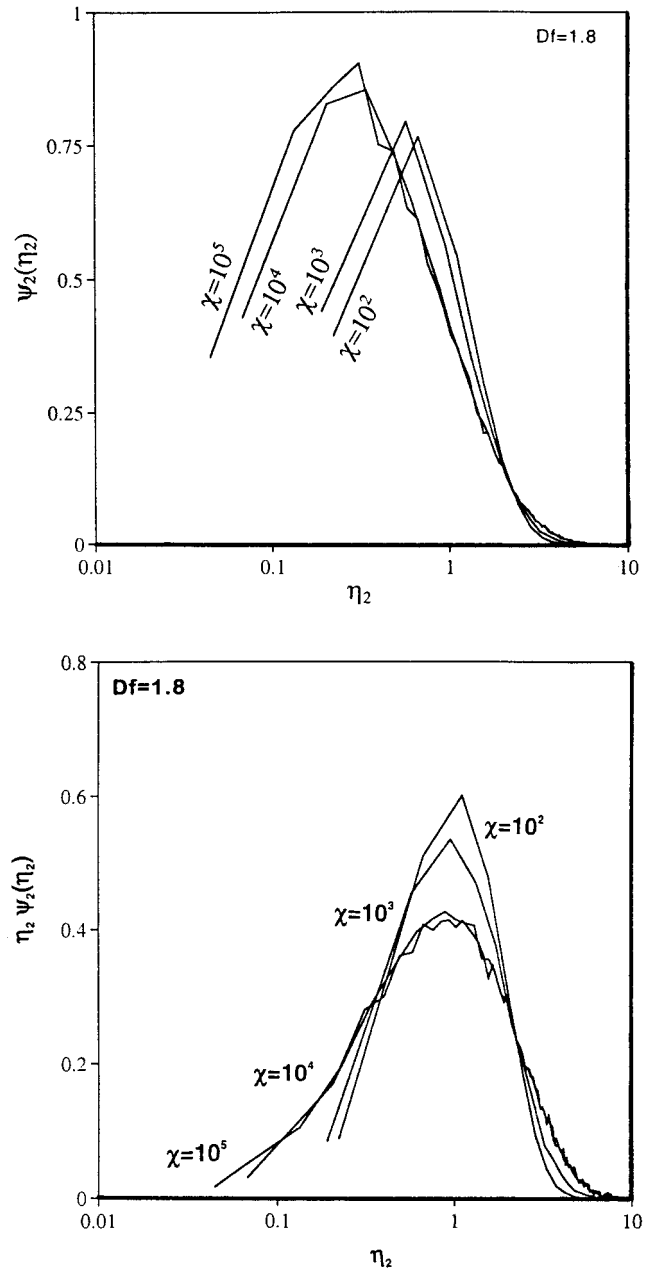

FIG. 7. Self-preserving distribution with respect to the surface area for different values of the dimensionless coalescence/coagulation time ratio parameter χ ($D_f = 1.8$); linearized coalescence rate law and Brownian coagulation in the continuum limit.

TABLE 3

Predicted Self-Preserving Spreads of Distributions with Respect to Surface Area of Populations Coagulating Due to Brownian Motion in the Continuum Regime, as Calculated by Monte Carlo Method: Dependence on the Characteristic Time Ratio χ

χ	$D_f = 2.5$	$D_f = 2.18$	$D_f = 1.8$
10^2	2.12	2.10	2.10
10^3	2.26	2.25	2.22
10^4	2.66	2.73	2.79
10^5	2.73	2.82	2.88

equation (PBE) (symbolically a balance between the accumulation, convection, coagulation, growth, and diffusion terms) with multi-internal variables and full coupling between the rate processes and both state variables. We are developing such methods for simulating particle generation–evolution in flames, exploiting the fact that in the generalized population balance equation (an integro-differential equation), the coagulation (integral part) term can be modeled using convenient Monte Carlo methods, while the other terms (differential) are modeled deterministically. This hybrid scheme will be recognized as similar in philosophy to the successful simulation of the ideal gas Boltzmann equation (another type of integro-differential equation) by the direct simulation Monte Carlo method (see, e.g., Refs. 3 and 26).

5. CONCLUSIONS, IMPLICATIONS, AND FUTURE WORK

We have presented here a Monte Carlo method to simulate the self-preserving distribution (with respect to both particle size and surface area) of a population of fractal aggregates undergoing simultaneous Brownian coagulation and finite-rate restructuring (coalescence) in the continuum regime. For simplicity, and to illustrate our methods, we assume that particle area does not explicitly influence the coagulation frequency and that the fractal dimension is an independently specified morphological parameter so that $\psi_1(\eta_1)$ is not influenced by the restructuring process. The formally predicted distributions with respect to size are found to be relatively insensitive to prespecified aggregate fractal dimension, becoming only slightly narrower with a decrease in the fractal dimension. Results from our MC simulations are independently checked with a finite-difference solution of the governing integro-ordinary differential equation in the self-preserving limit. The results from these methods are in excellent agreement. Size spread σ_g values were also calculated for initially log-normal distributions, formally assuming log-normality at all times during coagulation. While found to be systematically smaller than those obtained from MC and finite-difference numerical calculations, each of these three methods leads to the same potentially important conclusion, viz., in the continuum (high pressure) limit, the spread of coagulation-aged populations with respect to the size is nearly the same irrespective of aggregate fractal dimension. This is in sharp contrasts to the situation in the free-molecular limit, for which similar methods recently demonstrated a considerable broadening of coagulation aged population with reduced aggregate fractal dimension (59).

Subject to the above-mentioned uncoupling approximations, the distribution with respect to surface area is also found to be relatively insensitive to aggregate fractal dimension but, as expected, is highly sensitive to the characteristic time ratio (fusion/coagulation time): χ with broadening associated with slower relative coalescence rates. Thus, for $D_f = 3$, the distribution spread increased from a value of about 2.1 for $\chi = 100$ to a value of 2.9 for the slower coalescence case: $\chi = 10^5$

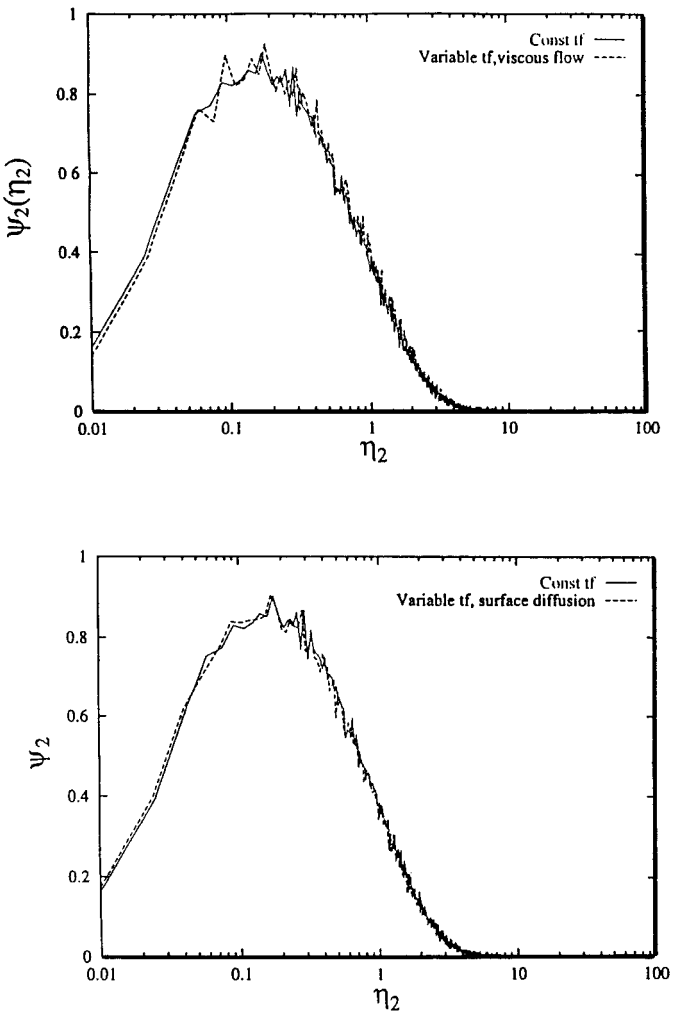

FIG. 8. Unconditional self-preserving distribution with respect to surface area (solid), formally allowing the characteristic fusion time, t_f, to vary according to the instantaneous value of the particle diameter $6v/a$, for (A) viscous flow sintering (dashed), and (B) surface-diffusion sintering rate laws (dashed); $D_f = 2.5$, $(\chi)_{t=0} = 100{,}000$.

TABLE 4

Asymptotic Value of Area Ratio Parameter, $\bar{a}/a_{ref}(\bar{v})$, as a Function of Fractal Dimension, D_f, and Characteristic Time Ratio, χ: Continuum Brownian Coagulation

	$\chi = 10^2$	$\chi = 10^3$	$\chi = 10^4$	$\chi = 10^5$
$D_f = 1.8$	0.928	1.08	3.03	4.64
$D_f = 2.18$	0.932	1.078	3.54	6.35
$D_f = 2.5$	0.930	1.07	3.94	7.92

(Table 3). The time lag to reach the self-preserving distribution with respect to area will be considered in future work from this laboratory. When generalized to incorporate coupled sintering rate results (e.g., Ref. 45) surface area distribution results can be used along with the methods discussed in Ref. 33 to predict the accessible surface area–volume and sorptive capacities of populations of fractal aggregates.[10] Such results will also be useful in determining the sizes and distribution of primary particles (spherules) in the aggregates, especially important for pigment particles. Also reported here for the first time is the self-preserving joint pdf between particle volume and area, a function that will be needed, among other things, to guide the development of moment methods for solving PBEs with two "internal" variables.

With regard to alternate computational techniques, we believe that Monte Carlo methods, applied here to the simplest case of spatially homogeneous coagulation with two particle state variables, will provide powerful tools for solving coagulation equations in more complex engineering environments. This will be especially true in cases requiring multi-internal variables (>2), where conventional finite-difference–sectional methods become computationally prohibitive.

We conclude by emphasizing that knowledge of coagulation-aged aggregate population size and area distributions over a range of Knudsen numbers will ultimately enable a number of technologically important predictions, including:

- deposition rates to immersed or containment solid surfaces from coagulating populations across laminar or turbulent boundary layers (30, 34, 47);
- accessible surface areas of coagulating restructuring populations including the apparent loss of accessible area of coagulating populations with time because of intra-aggregate diffusional limitations (33);
- radiation properties of coagulating, restructuring populations of aggregated particles (18);
- granular deposit microstructure and associated thermophysical properties resulting from the capture of aggregates from suspensions (50).

For the case of a coagulation rate constant independent of particle surface area, and constant fusion time, we have sought and found self-preserving solutions. But these interim idealizations must be relaxed to simulate systems of practical interest, especially those involving diffusional restructuring mechanisms shown earlier to be more sensitive to spherule size. Relaxation of these assumptions will inevitably lead to situations where self-preserving solutions are no longer obtainable. However, our methods still apply to these situations and could be used for predicting the evolution of aggregating populations without prespecifying the morphological parameter D_f. The Monte Carlo method, illustrated here for the simple case of spatially homogeneous coagulation with simultaneous coalescence, can readily be generalized to simulate particle population behavior in boundary layers and mixing layers, where local effects of convection, diffusion, and nucleation may be simultaneously important. In such situations, for solving the generalized population balance equation, the coagulation term would be modeled stochastically while the other terms would be modeled deterministically. This approach is currently being used to simulate experimental data for alumina particle production, growth, and transport in laminar counterflow diffusion flames (51, 52, 53). The Monte Carlo method can also be generalized to include more than the two particle state variables (e.g., chemical composition, etc.) in our analysis.

This paper is part of a longer range program to provide design tools for rational *sol reaction engineering*, as part of which efficient methods to simulate aggregate particle dynamics are urgently needed. The methods discussed here,

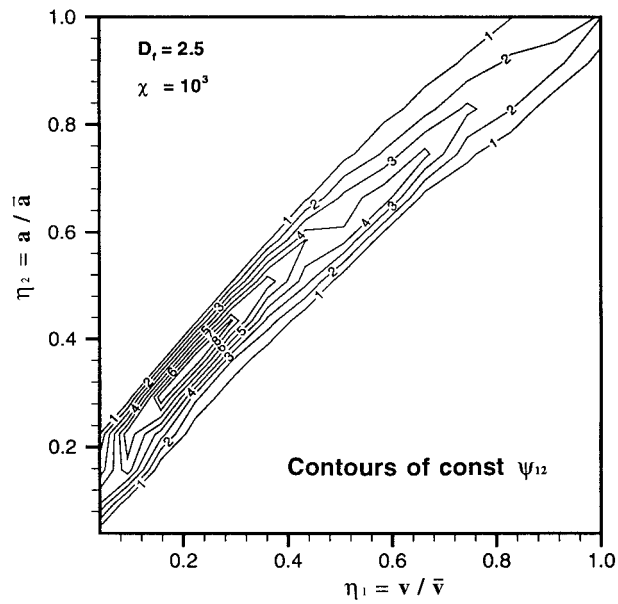

FIG. 9. Behavior of the self-preserving joint probability distribution function $\psi_{12}(\eta_1, \eta_2)$ for the particular case of coalescence/coagulation time ratio of 1000 and $D_f = 2.5$.

[10] Accessible area determines the utility of populations of aggregates as sorbents, rheological additives, etc.

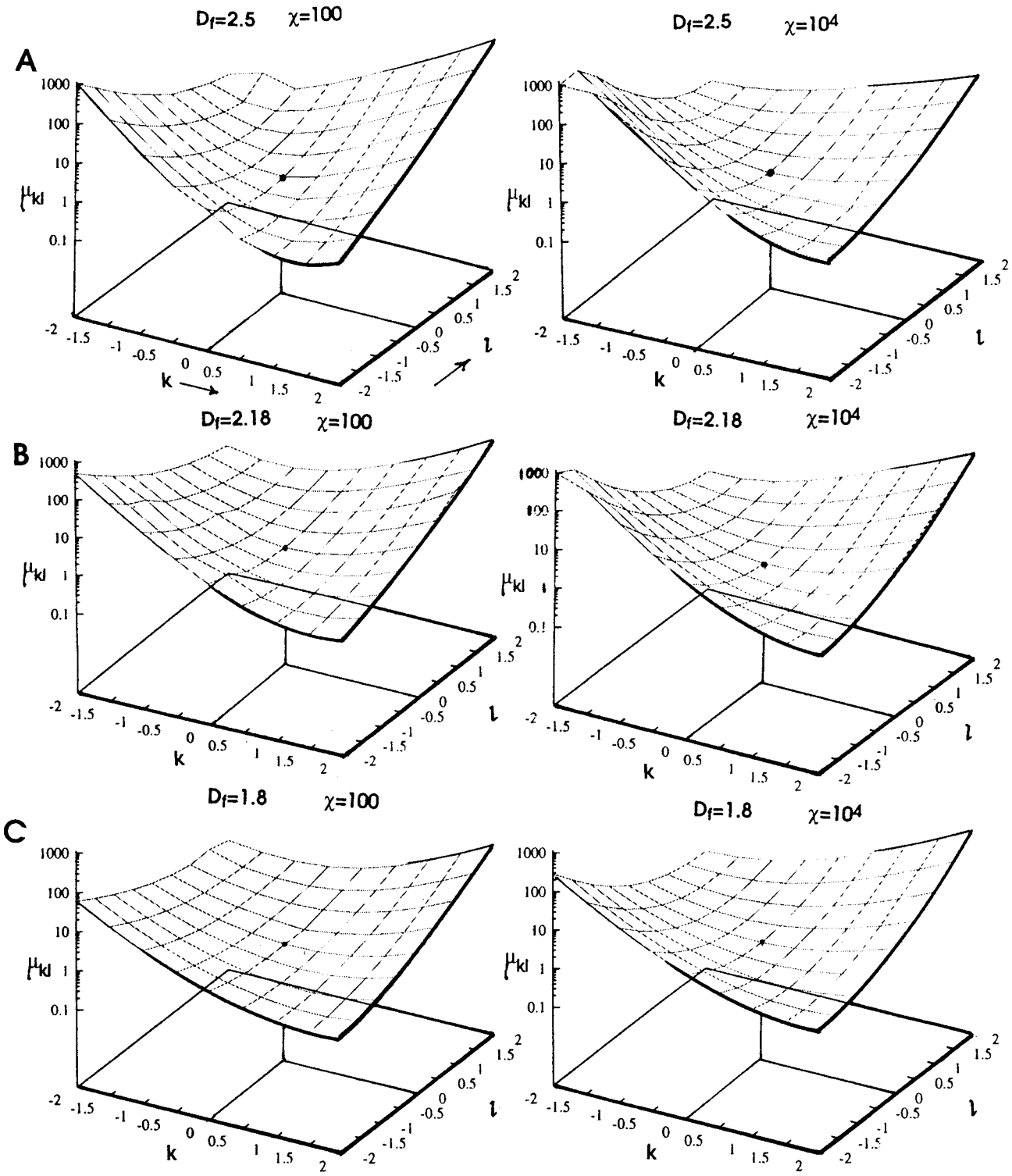

FIG. 10. Mixed k-l dimensionless moments, $\mu_{k,l}$ (cf. Eq. [23]), of the joint *probability density function* $\psi_{12}(\eta_1, \eta_2)$ for $-2 \leq k \leq 2$, $-2 \leq l \leq 2$.

along with extensions in progress motivated by comparisons with laboratory experiments, will find applications in controlling the synthesis of valuable powders and predicting and optimizing particle deposition rates from flow aggregate-laden gases in many situations of technological importance.

APPENDIX: NOMENCLATURE

a	Surface area of an aggregate
a'''	Total surface area per unit volume ($=N_p\bar{a}$)
a_1	Surface area of a spherule (primary particle)
$\bar{a}$	Mean surface area of the aggregate distribution
D_f	Aggregate fractal dimension
D_v	Bulk diffusion coefficient
D_s	Surface diffusion coefficient on nanoparticles
K	Proportionality constant in the coagulation kernel equation ($=2k_BT/(3\mu_{gas})$
k_B	Boltzmann constant
N_{prim}	Number of spherules in an aggregate
N_p	Aggregate number density
n	Aggregate number distribution function
r	Distance from aggregate center-of-mass
R_1	Primary particle radius
R_g	Aggregate radius of gyration
T	Absolute temperature
t_f	Characteristic time for spherule fusion
v	Volume of all condensed material in an aggregate
v_1	Volume of a primary particle (spherules)
v_m	Molecular volume (of monomer)
$\bar{v}$	Mean volume of the aggregate population

Greek

β	Aggregate–aggregate collision rate constant
χ	Ratio of characteristic fusion time to characteristic aggregate coagulation time
ϕ	Volume fraction of aerosol population
η_1	Similarity transformed *volume* variable, $v/\bar{v}$
η_2	Similarity transformed *area* variable, $a/\bar{a}$
μ	Viscosity of condensed material
μ_{gas}	Newtonian viscosity of carrier gas
$\mu_{k,l}$	Dimensionless "mixed" moment defined by Eq. [23]; see also Fig. 10
θ	Step function (Heaviside)
σ	Surface tension (energy) of the spherules
$\sigma_{g,v}$	Standard deviation of the distribution with respect to size
$\sigma_{g,a}$	Standard deviation of the distribution with respect to surface area
ψ_1	Dimensionless pdf with respect to particle volume; Eq. [14]
ψ_2	Dimensionless pdf with respect to surface area; Eq. [14]
ψ_{12}	Dimensionless joint pdf with respect to particle volume and surface area; Eq. [14]

ACKNOWLEDGMENTS

This research was supported in part by AFOSR (Grant 97-1-0266), NSF (Grant CTS-9871885), and Yale HTCRE Industrial Affiliate, duPont. We have also benefitted from useful discussions and correspondence with Drs. J. L. Castillo, P. Garcia-Ybarra, A. G. Konstandopoulos, T. Matsoukas, A. V. Filippov, S. Yu, Y. Xing, and R. B. Diemer Jr. A brief summary (extended abstract) of this work was presented as Paper #157h at AIChE'97, Los Angeles, CA, November 1997.

REFERENCES

1. Akhtar, M., Lipscomb, L., and Pratsinis, S. E., Monte-Carlo Particle Coagulation and Sintering, *Aerosol Sci. Tech.* **21,** 83 (1994).
2. Allen, M. P., and Tildesley, D. J., "Computer Simulations of Liquids," Oxford Univ. Press, Oxford, 1991.
3. Bird, G. A., "Molecular Gas Dynamics," Oxford Univ. Press, Oxford, 1992.
4. Cohen, R. D., The probability of capture and its impact on the Floc structure, *J. Chem. Soc. Faraday Trans. II* **85,** 1487 (1989).
5. Cohen, R. D., Rosner, D. E., and Tandon, P., "Kinetics of Restructuring of Large Multi-Particle Aggregates," AAAR Paper 8D4, 1993; Manuscript in preparation, 1999.
6. Diemer, R. B., and Olson, J., Representation of Particle Surface Area as a Function of Particle Mass in Evolving Aerosols Undergoing Coagulation and Breakage, Paper 106f, AIChE Annual Mtg., Chicago, 1996.
7. Friedlander, S. K., "Smoke, Dust and Haze," Wiley, New York, 1977.
8. Friedlander, S. K., and Wang, C. S., The self-preserving particle size distribution for coagulation by Brownian diffusion, *J. Colloid Interface Sci.* **22,** 126 (1966).
9. Gillispie, D. T., An exact method for numerically simulating the stochastic coalescence process in a cloud, *J. Atmos. Sci.* **32,** 1977 (1975).
10. Gooch, J. R., and Hounslow, M. J., Monte-Carlo simulations of size enlargement mechanisms in crystallization, *AIChE J* **42,** No. 7, 1864 (1996).
11. Helble, J. J., and Sarofim, A. F., Factors determining the primary particle size of flame-generated inorganic aerosols, *J. Colloid Interface Sci.* **128,** 348 (1989).
12. Julien, R., and Meakin, P., Simple models for the restructuring of three-dimensional ballistic aggregates, *J. Colloid Interface Sci.* **127,** 265 (1989).
13. Koch, W., and Friedlander, S. K., The effect of particle coalescence on the surface area of a coagulating aerosol, *J. Colloid Interface Sci.* **140,** 419 (1990).
14. Koylu, U. O., Xing, Y., and Rosner, D. E., Fractal morphology analysis of combustion generated aggregates using angular light scattering and electron microscope images, *Langmuir* **11,** No. 12, 4848 (1995).
15. Landgrebe, J. D., and Pratsinis, S. E., Gas phase manufacture of particulates: Interplay of chemical reaction and aerosol coagulation in the free-molecular regime, *Ind. Eng. Chem/Res. (ACS)* **28,** 1474 (1989).
16. Lee, K. W., Chen, H., and Gieseke, J. A., Log normally preserving size distribution for Brownian coagulation in the free molecule regime, *Aerosol Sci. Tech.* **3,** 53 (1984).
17. Lehtinen, K. E. J., Windeler, R. S., and Friedlander, S. K., A note on the growth of primary particles in agglomerate structures by coalescence, *J. Colloid Interface Sci.* **182,** 606 (1996).
18. Mackowski, D. W., Tassopoulos, M., and Rosner, D. E., Effect of radiative heat transfer on the coagulation dynamics of combustion generated particles, *Aerosol Sci. Tech.* **20,** 83 (1994).
19. Martinez-Herrera, J., and Derby, J. J., Analysis of capillary driven viscous flows during the sintering of ceramic powders, *AIChE J.* **40,** No. 11, 1794 (1994).
20. Matsoukas, T., and Friedlander, S. K., Dynamics of aerosol aggregate formation, *J. Colloid Interface Sci.* **146,** No. 2, 495 (1991).
21. Meakin, P., The growth of fractal aggregates, *in* "Time-Dependent Effects in Disordered Materials" (R. Pynn, and T. Riste, Eds.), pp. 45–70. Plenum Press, New York/London, 1987.
22. Megaridis, C. M., and Dobbins, R. A., Morphological description of flame-generated materials, *Comb. Sci. Tech.* **71,** 95 (1990).
23. Mullins, M. W., Mass transport at interfaces in single component systems, *Metal. Mater. Trans. A* **26,** 1917 (1995).

24. Nyeki, S., and Colbeck, I., Fractal dimension analysis of single, *in situ*, restructured carbonaceous aggregates, *Aerosol Sci. Tech.* **23,** 109 (1993).
25. Oh, C., and Sorensen, C. M., Light scattering study of fractal cluster aggregation near the free-molecular regime, *J. Aerosol Sci.* **28,** No. 6, 937 (1997).
26. Papadopoulos, D. H., and Rosner, D. E., Enclosure gas flows driven by non-isothermal walls, *Phys. Fluids* **7,** No. 11, 2535 (1995).
27. Potanin, A. A., On computer simulation of the deformation and breakup of colloidal aggregates in shear flow, *J. Colloid Interface Sci.* **157,** 399 (1993).
28. Raabe, O. G., Particle size analysis utilizing grouped data and the log-normal distribution, *J. Aerosol Sci.* **2,** 289 (1971).
29. Randolph, A. D., and Larson, M. A., "Theory of Particulate Processes," 2nd ed. Academic Press, New York, 1988.
30. Rosner, D. E., Total mass deposition rates from polydispersed aerosols, *AIChE J.* **35,** No. 1, 164 (1989).
31. Rosner, D. E., Yu. S., and Tandon, P., Vapor scavenging and mass deposition rates of coagulation-aged populations of non-spherical particles distributed with respect to both particle volume and surface area, in preparation, 1999.
32. Rosner, D. E., and Tandon, P., Accessible surface area/volume and sorptive capacity of populations of 'micro-porous' particles (aggregates) distributed with respect to both size and shape, prepared for submission, 1999.
33. Rosner, D. E., and Tandon, P., Prediction and correlation of accessible area of large multi-particle aggregates, *AIChE J.* **40,** No. 7, 1167 (1994).
34. Rosner, D. E., and Tassopoulos, M., Deposition rates from polydispersed particle populations of arbitrary spread, *AIChE J.* **35,** 1497 (1989).
35. Rosner, D. E., Mackowski, D. W., Tassopoulos, M., Castillo, J. L., and Garcia Ybarra, P., Effects of heat transfer on the dynamics and transport of small particles in gases, *I/EC Res.* **31,** 760 (1992).
36. Schaefer, D. W., Fractal models and structure of materials, *MRS Bull.* **8,** No. 2, 22 (1988).
37. Schmidt-Ott, A., *In situ* measurement of fractal dimensionality of ultrafine aerosol particles, *Appl. Phys. Lett.* **52,** No. 12, 954 (1988).
38. Schumann, T. E. W., Theoretical aspects of the size distribution of fog particles, *Quart. J. Roy. Meteor. Soc.* **66,** 195 (1940).
39. Smoluchowski, M. von, Versuch einer Mathematischen Theorie der Koagulationskinetic Kollider Losungen, *Z. Phys. Chem.* **92,** 129 (1917).
40. Smith, M., and Matsoukas, T., Constant-number Monte-Carlo simulation of population balances, *Chem. Eng. Sci.* **53,** No. 9, 1777 (1998).
41. Sorenson, C., Cai, J., and Lu, N., Light scattering measurements of monomer size, monomers per aggregate, and fractal dimension for soot aggregates in flames, *Appl. Optics* **31,** 6547 (1992).
42. Spouge, J. L., Monte-Carlo result for random coagulation, *J. Colloid Interface Sci.* **107,** 38 (1985).
43. Swift, D. L., and Friedlander, S. K., The coagulation of hydrosols by Brownian motion and laminar shear flow, *J. Colloid Interface Sci.* **19,** 621 (1964).
44. Tandon, P., "Transport Theory for Particles Generated in Combustion/CVD Environments," PhD Dissertation, Department of Chemical Engineering, Yale Univ., New Haven, CT, 1995.
45. Tandon, P., and Rosner, D. E., Sintering kinetics and transport evolution of large multi-particle aggregates, *Chem. Eng. Comm.* **151,** 147 (1996).
46. Tandon, P., and Rosner, D. E., Translational Brownian diffusion coefficient of large (multi-particle) aggregates, *I/EC Res.* **34,** No. 10, 3265 (1995). [Our pseudo-homogeneous mathematical model/finite-analytical computational technique has also been used, seemingly independently, by S. Veerapaneni, and M. R. Weisner, *J. Colloid Interface Sci.* **177,** 45 (1996)]
47. Tandon, P., and Adewumi, M. A., Particle deposition from turbulent flow in a pipe, *J. Aerosol Sci.* **29,** Nos. 1–2, 141 (1998).
48. Tandon, P., and Rosner, D. E., Kinetics of multi-particle fractal aggregates undergoing surface and bulk diffusion sintering, in preparation, 1997.
49. Tandon, P., Yu, S., and Rosner, D. E., Monte-Carlo simulation of particle generation, morphological evolution and transport in laminar counterflow diffusion flames, in preparation, 1999.
50. Tassopoulos, M., and Rosner, D. E., Microstructural descriptors characterizing granular deposit, *AIChE J.* **38,** No. 1, 15 (1992).
51. Xing, Y., Koylu, U. O., Rosner, D. E., Synthesis and restructuring of inorganic nanoparticles in counterflow diffusion flames, *Combustion and Flame* **107,** 85 (1996).
52. Xing, Y., Rosner, D. E., Koylu, U. O., and Tandon, P., Morphological evolution of oxide nano-particles in laminar counterflow diffusion flames—measurements and modeling, *AIChE J.* **43,** No. 11A, 2641 (1997).
53. Xing, Y., Koylu, U. O., Tandon, P., and Rosner, D. E., Measuring and modeling the synthesis and morphological evolution of particles in counterflow diffusion flames, *in* "Proc. Fifth World Congress of Chemical Engineering, AIChE, San Diego, CA, July, 1996," Vol V, pp. 43–48, 1996.
54. Xing, Y., and Rosner, D. E., Surface melting of ultrafine particles: predicting spherule size in vapor phase nanometer particle formation, Paper V5.36, "Proc. Fall 1996 MRS Mtg.," p. 521 (1996) and Vol. 457, pp. 167–172 (1997). See, also, *J. Nanoparticle Res.* (Kluwer) (to appear, summer 1999).
55. Xing, Y., Koylu, U. O., and Rosner, D. E., *In situ* light scattering measurements of morphologically evolving flame-synthesized nano-aggregates, *Appl. Optics* in press, 1999.
56. Xiong, Y., and Pratsinis, S. E., Formation of agglomerate particles by coagulation and sintering: Part I-A, Two dimensional solution of the population balance equation, *J. Aerosol Sci.* **24,** No. 3, 283 (1993).
57. Vemury, S., and Pratsinis, S. E., Self-preserving distributions of agglomerates, *J. Aerosol Sci.* **26,** No. 2, 175 (1995).
58. Weber, A. P., and Friedlander, S. K., Determination of bond strength between nano-sized particles, "MRS Symp. Proceedings, San Francisco, 1994." [Note: From the viewpoint of Cohen, Rosner, and Tandon (5) what Weber and Friedlander originally reported as the spherule binding energy is, rather, an activation energy for "diffusive restructuring" (by rolling and/or sliding)-Private communication: D. E. Rosner to A. P. Weber dated Sept. 16, 1994. This viewpoint appears to have been accepted and incorporated in the most recent account of these experiments, *J. Aerosol Sci.* **28,** No. 2, 179 (1997)]
59. Wu, M. K., and Friedlander, S. K., Enhanced power law agglomerate growth in the free molecular regime, *J. Aerosol Sci.* **24,** No. 3, 273 (1993).